Catalysis Science & Technology

ROYAL SOCIETY OF CHEMISTRY

PAPER

View Article Online
View Journal

Cite this: DOI: 10.1039/d5cy01517k

Alginate-supported L-arginine as a biobased heterogeneous catalyst for the conversion of glycidol and CO_2 into glycerol carbonate

Tanika Kessaratikoon, [ab] Silvano Del Gobbo,[c] Valerio D'Elia [*bd] and Paolo P. Pescarmona [*a]

Glycerol carbonate is emerging as a safe and sustainable CO_2-based chemical with multiple attractive applications. Among various synthetic strategies, the preparation of glycerol carbonate from CO_2 and glycidol, a glycerol derivative, is an atom-economic, thermodynamically favourable process that does not require the use of sacrificial reagents. In this work, we report the rational design, synthesis and application of a novel biobased catalyst for this reaction, which was prepared by grafting L-arginine onto a sodium alginate support. This synthetic approach resulted in a heterogeneous, halide-free catalyst with the desirable combination of active sites (basic, nucleophilic sites and hydrogen bond donors) for glycidol activation, leading to much higher glycerol carbonate yield and selectivity compared to previously reported biobased heterogeneous catalysts for this reaction. The catalyst can operate under mild conditions (45–80 °C, 10–30 bar CO_2) and showed good recyclability. Careful physicochemical characterization by FTIR, NMR, XPS, TGA, elemental analysis and GPC allowed us to define the structure–activity relationships and to identify the suitable reaction conditions to prevent undesirable catalyst degradation processes such as active site hydrolysis and alginate decarboxylation. Overall, this work contributes to the development of a sustainable and safe catalytic process for the efficient conversion of biobased glycidol and CO_2 into glycerol carbonate, a product of growing importance.

Received 10th December 2025,
Accepted 2nd March 2026

DOI: 10.1039/d5cy01517k

rsc.li/catalysis

Introduction

Glycerol carbonate (GLC) is a renewable chemical with attractive physicochemical properties, low flammability, and a wide range of applications.[1,2] It is used as a non-toxic solvent for chemical[3] and electrochemical processes[4] and as an ingredient for various commercial formulations in cosmetic and healthcare products.[5] GLC also serves as a precursor of carbonate-based monomers, such as glycerol carbonate methacrylate[6,7] and of bis-carbonates that are typically used for the synthesis of isocyanate-free polyhydroxyurethanes.[8–10] Synthetically, GLC can be regarded as the derivative of the condensation reaction of two renewable waste products, *i.e.*, glycerol from the biodiesel industry[11] and CO_2 from anthropogenic activities, thus offering a unique possibility to upcycle both chemicals into a value-added product.

Based on such attractive properties, the development of efficient and sustainable synthetic routes to GLC is receiving increasing attention.[12–14] The direct coupling of CO_2 and glycerol, although highly desirable, is a thermodynamically unfavourable process that proceeds with very low yields,[15] unless overstoichiometric sacrificial reagents are added as dehydrating agents.[16] An alternative pathway is the reaction of glycerol with carbonylation agents such as dimethyl carbonate[17] or urea.[18] Although this approach is effective, it suffers from poor atom economy due to by-product formation (methanol or ammonia), and the carbonylation agent is generally used in a large excess to shift the equilibrium towards the products. A different, promising atom-economic strategy, using CO_2 as a substrate, is the cycloaddition of CO_2 to glycidol.[12] The latter substrate can be derived from glycerol through different routes.[19]

Typically, the cycloaddition of CO_2 to epoxides requires binary or dual-component catalytic systems including a moiety for the activation of the epoxide (a H-bond donor or a metal centre) and a nucleophilic species for its ring-opening (typically a halide anion).[21–23] Producing such multifunctional catalytic

[a] *Engineering and Technology Institute Groningen (ENTEG), University of Groningen (RUG), Nijenborgh 3, 9747 AG Groningen, The Netherlands. E-mail: p.p.pescarmona@rug.nl*
[b] *School of Molecular Science and Engineering (MSE), Vidyasirimedhi Institute of Science and Technology (VISTEC), Wangchan Valley 555 Moo 1 Payupnai, Wangchan, Rayong 21210, Thailand. E-mail: valerio.delia@vistec.ac.th*
[c] *Italian National Agency for New Technologies, Energy and Sustainable Economic Development (ENEA), Via Anguillarese 301, 00123 Roma, Italy*
[d] *Department of Biological and Environmental Sciences and Technologies (DiSTeBA), University of Salento, Ecotekne SP 6, 73047 Monteroni di Lecce, Italy. E-mail: valerio.delia@unisalento.it*

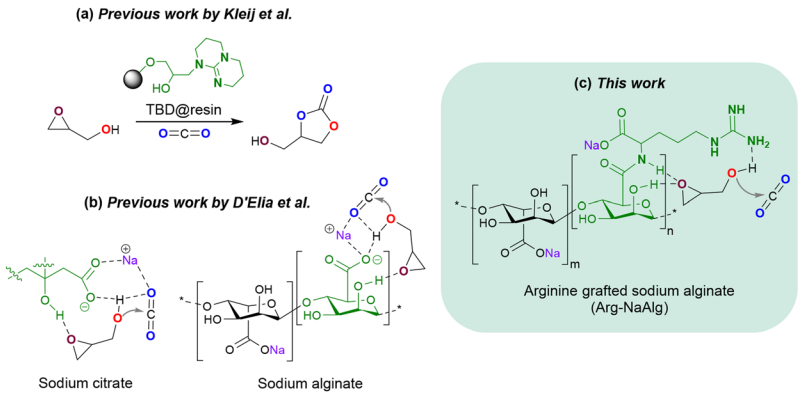

Scheme 1 (a) Cycloaddition of CO_2 to glycidol catalyzed by superbase TBD (1,5,7-triazabicyclo[4.4.0]dec-5-ene) supported on Merrifield resin (TBD@resin).[14] (b) Proposed mechanism of substrate activation and coordination in the cycloaddition of CO_2 to glycidol by homogeneous (sodium citrate) and heterogeneous (sodium alginate) biobased catalysts.[20] (c) Proposed activation of glycidol for the cycloaddition reaction with CO_2 by the biobased catalyst reported in this work.

systems in the heterogeneous form is often a complex endeavour requiring the co-immobilization of two different catalytic components in a suitable geometric arrangement[24] through multiple synthetic steps[25] and/or through the use of toxic and environmentally hazardous[26] organic halogenides.[27] However, in the specific case of α-epoxy alcohol substrates, such as glycidol, while the traditional halide-based catalytic approach is efficient,[28,29] the cycloaddition reaction of CO_2 can also proceed through an alternative substrate-specific mechanism that does not require the presence of halide nucleophiles[27] and that can be catalyzed by a Lewis acidic metal complex[30,31] or an organic base[32] (Scheme 1a). It has been proposed that the base-catalyzed mechanism proceeds through activation of the hydroxyl group, enabling its oxygen to attack CO_2 to form a hemicarbonate intermediate (Scheme 2). This intermediate then acts as a nucleophile to open the epoxide ring, followed by proton transfer, ultimately yielding glycerol carbonate.[12]

The state-of-the-art heterogeneous catalyst for this reaction consists of organic superbases immobilized on polymer beads (TBD@Merrifield, Scheme 1a), which can operate in a continuous flow reactor.[14] Recent years have witnessed a growing interest in advancing organocatalysts for CO_2 conversion through the development of biobased catalytic systems.[33–37] These are considered as inherently sustainable, nontoxic, and readily available.[38] In this context, it has been shown that GLC formation from CO_2 and glycidol can be catalyzed by simple biobased compounds such as sodium citrate in the homogeneous phase and sodium alginate (NaAlg) as a heterogeneous catalyst.[20] Based on different experimental evidence, it was proposed that these compounds catalyze the cycloaddition of CO_2 to glycidol by virtue of the simultaneous presence of mild basic sites (sodium carboxylates) and H-bonding sites for the activation of glycidol and coordination of the substrates (Scheme 1b). However, the catalytic performance of NaAlg as a heterogeneous catalyst was moderate and required long reaction times (typically 24 h) and a high catalytic loading (10 wt%) to achieve high substrate conversions. Against this backdrop, we reasoned that the functionalization of alginates with biobased compounds bearing suitable active sites (basic moieties, H-bond donors) would lead to an improved catalytic performance in the cycloaddition of CO_2 to glycidol while preserving the bioderived nature of the catalyst. In this work, this strategy was realized by functionalizing alginate biopolymers, extracted from seaweed, with L-arginine, a naturally occurring amino acid endowed with a basic functionality (guanidine group) and H-bonding moieties (Scheme 1c). The resulting catalyst could efficiently promote the cycloaddition of CO_2 to glycidol yielding GLC by using low catalytic loading (1.5 and 3 wt%) in short reaction times (3 h). Additionally, the catalytic system showed good recyclability and an environment-friendly profile based on its fully biobased nature. Moreover, it strongly enhanced the catalytic performance compared to previously reported biobased heterogeneous catalysts for the same application.

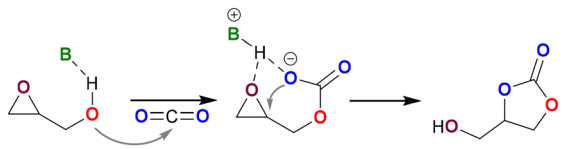

Scheme 2 Proposed mechanism for the reaction of CO_2 with glycidol to produce glycerol carbonate *via* a proton-shift mechanism catalyzed by organic bases (B).

Results and discussion

Immobilization of amino acids on sodium alginate (AA-NaAlg)

With the purpose of developing a fully biobased heterogeneous catalyst with basic active sites and hydrogen bond donor moieties for the coupling of glycidol and CO_2 (Scheme 1c), the immobilization of three amino acids carrying basic groups (arginine, lysine, and histidine, see Fig. 1) on sodium alginate (NaAlg) was investigated. The sodium alginate biopolymer consists of mannuronate (M) and guluronate (G) units,[39] which are present in an M/G = 1.56 ratio, as determined by ^{1}H NMR

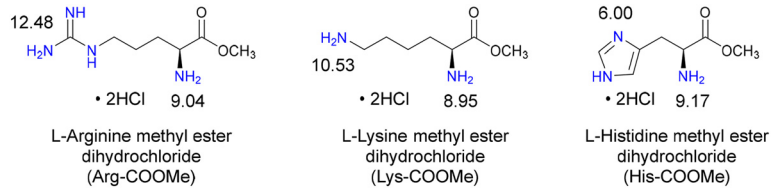

Fig. 1 Amino acid precursors used in the synthesis of the catalyst. The pK_a values for the amino acid form of these compounds are shown next to each basic group.[41]

(Fig. S1, SI). The grafting was carried out by adapting a previously reported procedure by Labre *et al.*,[40] which was carried out in $(NH_4)_2CO_3$ buffer to maintain a basic environment (pH = 8–9).

At small scale, both arginine methyl ester (Arg-COOMe) and lysine methyl ester (Lys-COOMe) were successfully immobilized onto sodium alginate (as shown by ^{1}H NMR in Fig. S2 and S3, SI). However, the grafting of histidine methyl ester (His-COOMe) was unsuccessful under the tested conditions (Fig. S4, SI), possibly due to the steric hindrance caused by the imidazole group, which is located in proximity of the α-amino group through which the grafting to the alginate should take place. The unsuccessful immobilization was corroborated by the presence of the unreacted activated ester obtained by reaction of alginate with DMTMM, as indicated by a singlet at 3.96 ppm corresponding to the methyl groups of the triazine ester[42] in the ^{1}H NMR spectrum of His-NaAlg (Fig. S4, SI).

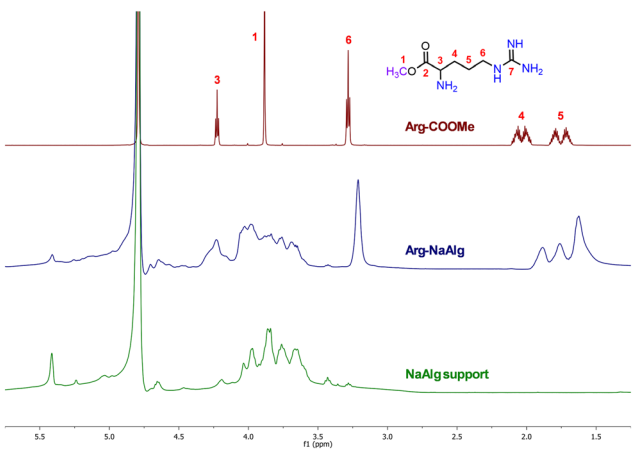

Fig. 2 ^{1}H NMR spectra of Arg-COOMe (top), of the NaAlg support (bottom), and of the synthesized Arg-NaAlg (middle).

Upon catalyst synthesis upscaling, Lys-COOMe consistently led to the formation of a gel-like material (Fig. S5, SI), which hindered workup and utilization. This gel formation may be attributed to the primary amino side chain of lysine, which could engage in additional covalent (deprotonated) or electrostatic (protonated) interactions with the carboxylate groups of alginate, which could lead to crosslinking and gelation.[43] The different reactor configuration used in the upscaled synthesis (see Experimental section) might have promoted the gelation compared to the small-scale method. Different from what was observed with Lys-COOMe, the upscaled immobilization procedure was effective with Arg-COOMe, as shown by FTIR (Fig. S6, SI) and ^{1}H NMR (Fig. 2 and S7, SI) spectroscopy. Therefore, further experiments were conducted using only alginate-supported arginine methyl ester (Arg-NaAlg). In the $(NH_4)_2CO_3$ buffer used to immobilize the amino acids, the α-amino groups of the arginine molecules (in their methyl ester form, Arg-COOMe) are expected to be in their deprotonated form, thus enabling the amidation with the DMTMM activated carboxylate groups of NaAlg. On the other hand, the guanidino group (see Fig. 1 for the pK_a) of Arg-COOMe is expected to be mainly in its protonated form due to stabilization through resonance between the three neighbouring amino groups (Scheme 3).[41,44] Based on these considerations, the grafting of the amino acid onto alginate should occur mainly through the α-amino groups. The expected structure of Arg-NaAlg is shown in Scheme 3.

The upscaled Arg-NaAlg was characterized through a combination of techniques to ascertain the immobilization of arginine on sodium alginate. The ^{1}H NMR spectrum of the upscaled Arg-NaAlg measured in D_2O (Fig. 2), in which the material is soluble, corresponds to that of the small-scale counterpart (Fig. S2, SI). The successful immobilization is indicated by the peaks of protons in positions 3, 4, 5, and 6

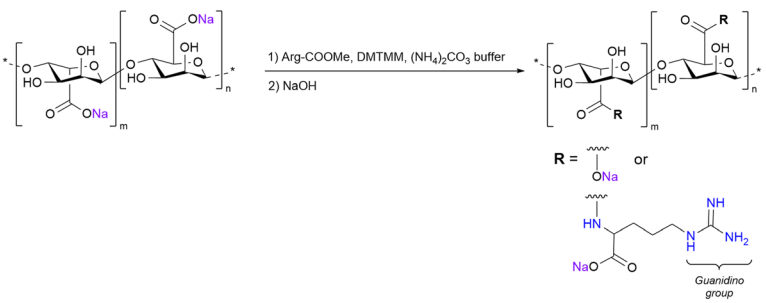

Scheme 3 Procedure for the immobilization of Arg-COOMe on NaAlg.

of Arg-COOMe in the spectrum of Arg-NaAlg, with the signals being slightly shifted and significantly broadened compared to the free Arg-COOMe molecule. It is worth noting that the peak of the methyl group of the ester of Arg-COOMe is not visible in the spectrum of Arg-NaAlg, either because it is absent or because it so small that it is covered by the broad alginate signal in that region. This suggests that during the immobilization process, most of the ester groups of the grafted Arg-COOMe are hydrolyzed. The characteristic broad peaks of the NaAlg support are all present in Arg-NaAlg, although the shape of the convoluted multipeak profile between 3.5 and 4.2 ppm slightly differs from that in the parent NaAlg. This can be attributed to the grafting of the arginine, as the peaks in this region are associated with the protons of the uronate rings (mannuronate and guluronate) of the alginate.[45]

Further insight into the structure of Arg-NaAlg was provided by ^{13}C NMR (Fig. 3). Overall, the carbon signals of the arginine moiety shifted after the immobilization step, suggesting successful grafting on sodium alginate. In particular, the carbonyl carbon (2) of the carboxylate group shifted significantly downfield to 177.8 ppm and showed a distinct decrease in intensity compared to the 169.6 ppm peak of carbonyl carbon in the L-arginine methyl ester (Arg-COOMe), suggesting conversion of the ester group into a sodium carboxylate (Scheme 3).[46] With the formation of this sodium carboxylate group, all the carbon atoms along the chain were deshielded.[47] The extent of the shift of the peaks compared to the free L-arginine methyl ester was used to determine in which position(s) the arginine was grafted through the formation of amide bonds. A clear shift downfield of the α-carbon peak of Arg-COOMe (3) from 52.9 ppm to 54.9 ppm indicates that NaAlg preferentially reacts with Arg-COOMe at the α-amino group rather than at the guanidino group, for which only a smaller shift from 156.0 ppm to 156.7 ppm was observed for the carbon peak at position 7.[47] This observation matches our expectation of a preferential grafting through the amino group connected to the α-carbon at the pH in which the immobilization was carried out (*vide supra*). The resonance stabilization of the guanidino group implies that the formation of an amide bond with NaAlg is less likely than with the α-amino group, which is a primary amine.[48] The new peak at 169.4 ppm in the spectrum of Arg-NaAlg (middle) stems from the carbonyl group of the amide bond formed with arginine species,[46] further confirming successful immobilization. Finally, the methyl carbon of the methyl ester (1) disappeared in the spectrum of Arg-NaAlg (middle) due to hydrolysis in the presence of NaOH.

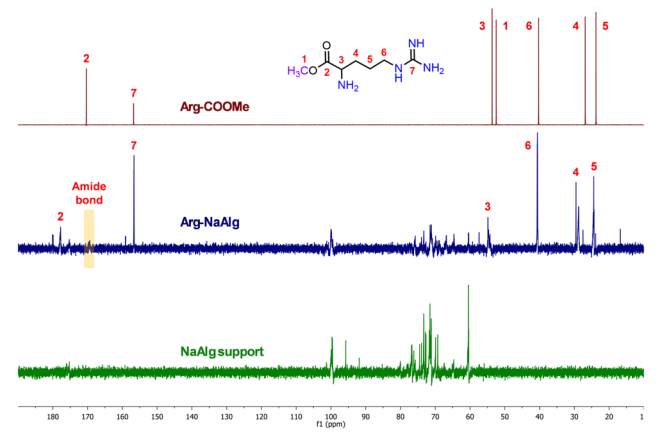

Fig. 3 ^{13}C NMR spectra of Arg-COOMe (top), of the NaAlg support (bottom), and of the synthesized Arg-NaAlg (middle).

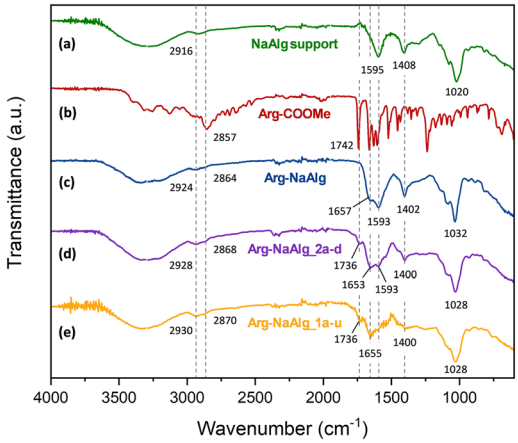

Fig. 4 FTIR spectra of (a) the NaAlg support, (b) Arg-COOMe, (c) the synthesized Arg-NaAlg, and the used Arg-NaAlg after 4 catalytic runs under conditions (d) 2a-d and (e) 1a-u.

The immobilization of Arg-COOMe onto NaAlg was also investigated by ATR-FTIR (Fig. 4). Arg-NaAlg (Fig. 4c) contained the three main peaks arising from the NaAlg support (Fig. 4a), which appear at 1032 cm^{-1} (C–O stretching of the pyranose ring), 1402 and 1593 cm^{-1} (C–O and C=O stretching of sodium carboxylate groups, respectively).[20,45] Slight shifts in the wavenumbers of the characteristic peaks of NaAlg and a shoulder peak at around 1657 cm^{-1} originating from C=O stretching of the formed amide bonds[40] further confirm successful immobilization. The absence of the signal at 1742 cm^{-1} in Arg-NaAlg, corresponding to the C=O stretching of the methyl ester of Arg-COOMe (Fig. 4b), confirms the hydrolysis of the ester group upon grafting.

Elemental analysis allowed estimating the degree of substitution (DS) of NaAlg with arginine moieties. The obtained DS value (46%, Table S3, SI) indicates that the Arg-NaAlg catalyst is rich in the desired active sites. This DS agrees well with literature results for the grafting of another amino acid (*e.g.*, L-alanine) on alginate oligosaccharides.[40] The prepared Arg-NaAlg catalyst was further characterized by high-resolution XPS (Fig. 5). The C 1s spectral region of Arg-NaAlg (Fig. 5a) shows four main components centred at 284.8 eV, 286.3 eV, 287.4 eV and 288.4 eV (Table S4, SI). Compared to the XPS spectrum of NaAlg reported in the literature,[20] the C 1s XPS spectrum of Arg-NaAlg shows an increase in the relative intensity of the component centred at 284.8 eV, which is attributed to sp^3-type carbon atoms of aliphatic C–C bonds. The increase in intensity of this component upon arginine

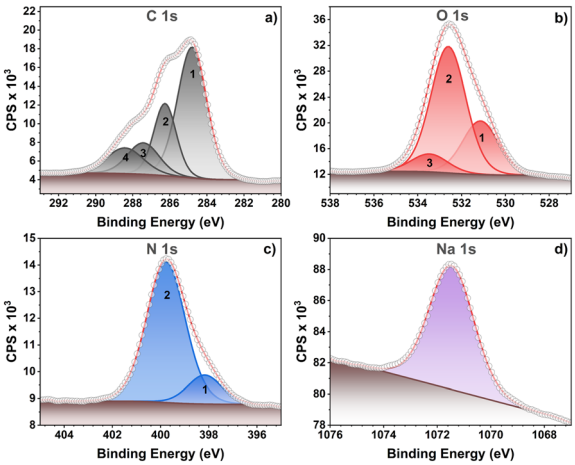

Fig. 5 High-resolution XPS spectra of Arg-NaAlg in the (a) C 1s, (b) O 1s, (c) N 1s and (d) Na 1s spectral regions.

grafting is in agreement with the introduction of several new C–C bonds due to the presence of the aliphatic side chain of arginine. Aside from this difference, the presence of arginine in Arg-NaAlg did not result in a significant variation in the position and identity of the fitted synthetic components compared to NaAlg. Indeed, the signals of the carbon atoms from the *C*–N and –N–*C*=O (amide) moieties and the guanidino group of the grafted arginine overlap with those of the NaAlg backbone. The binding energy of *C*–N-type carbon atoms in arginine, reported at about 286.0 eV,[49] overlaps with that of the *C*–O carbon atoms of NaAlg at about 286.0 eV,[20] giving rise to the signal observed at 286.3 eV for Arg-NaAlg (Table S4, SI). The amido carbon of the –N–*C*=O moiety of Arg is expected at 288.0–289.0 eV,[50] which is in the same region as the binding energy of the –O–*C*=O– signal of NaAlg (288.3 eV),[20] giving rise to a single component observed for Arg-NaAlg at 288.4 eV (Table S4).[51] Finally, the guanidine carbon, HN=*C*– (NH, NH_2), is expected to show a binding energy of *ca.* 287.7 eV,[49] which overlaps with the –O–*C*–O– carbon atoms of the NaAlg backbone at *ca.* 287.6 eV[20] (component observed at 287.4 eV in Arg-NaAlg, Table S4). The high-resolution O 1s XPS signal of Arg-NaAlg (Fig. 5b) shows components centred at 531.1 eV, 532.6 eV and a minor peak at 533.5 eV (Table S4). The components at 531.1 eV and 532.6 eV, with peak intensity ratio close to 1 : 2, are in good agreement with the literature-reported spectrum of NaAlg[52] and are attributed, respectively, to oxygen atoms of the sodium carboxylate group (*COO*Na) and to the C–*O*–R (R = C, H) moieties[53] of the alginate backbone. Additionally, the former component should overlap with the peak of the *O*=C–OH moiety of the grafted arginine (expected at 530.8–531.9 eV in amino acids).[49] The broad minor component at 533.5 eV may indicate the presence of weakly adsorbed oxygen species and moisture in the sample.[54] The appearance of a signal centred at about 400 eV (Fig. 5c) in the XPS spectrum is consistent with the grafting of arginine as observed by NMR and FTIR investigations. Analysis of the high-resolution N 1s spectrum (Fig. 5c) shows a main peak at 399.8 eV, as expected based on the presence of the protonated guanidinium group and of the amido nitrogen (*N*–C=O), which have been reported to occur at about 400 eV.[55] A minor component at particularly low binding energies (398.2 eV) is consistent with the presence of imine-type nitrogen atoms (C=*N*H)[55,56] and may derive from the presence of unprotonated guanidine moieties. Finally, the XPS spectrum shows the presence of sodium cations based on a peak centred at 1071.5 eV, which is similar to that observed in the XPS spectrum of unfunctionalized NaAlg,[20] showing that the alginate backbone of Arg-NaAlg bears unprotonated sodium carboxylate groups. Additionally, it is worth noting that a broad scan survey spectrum of Arg-NaAlg did not reveal the presence of chlorine, if not in very minor amounts, close to the detection limit (Fig. S8 and S9). This indicates that the initial hydrochloride salts of Arg-COOMe underwent neutralization (as supported by the successful Arg grafting and by the presence of unprotonated guanidine moieties discussed above) and/or anion exchange with hydroxy and hydrogen carbonate anions.

Further characterization of the Arg-NaAlg catalyst was carried out by gel permeation chromatography (GPC), which allowed investigating whether the grafting procedure altered the molecular weight of the NaAlg support (Table S6 and Fig. S11, SI). Sodium alginate is a biobased polymer with a high weight-average molecular weight (M_w = 221 800 g mol^{-1}) and a broad distribution of chain lengths, as reflected by its high dispersity value ($Đ$ = 76). After modification of NaAlg with arginine, the weight-average molecular weight decreased (M_w = 53 020 g mol^{-1}) and the distribution of chain length became narrower as indicated by the lower dispersity value ($Đ$ = 9). The decrease in M_w is attributed to partial hydrolysis of the high-molecular-weight NaAlg chains under the mildly basic conditions (pH 8–9) used during the prolonged immobilization step (16 h), generating shorter fragments.[57] On the other hand, the number-average molecular weight (M_n) of Arg-NaAlg approximately doubled relative to pristine NaAlg, which is consistent with the successful incorporation of arginine units and an overall increase in the average molecular weight per chain, but probably also stems from loss of the lower-molecular-weight alginate oligomers during the washing steps of the grafting protocol. The combination of the lower M_w value and higher M_n value in Arg-NaAlg compared to NaAlg leads to a narrower molecular-weight distribution and thus to the lower dispersity.[58]

Collectively, these observations indicate simultaneous grafting of arginine species and partial degradation of the higher-molecular-weight alginate chains under the applied immobilization protocol.

Next, we assessed the thermal stability of the Arg-NaAlg catalyst and of the NaAlg support by thermogravimetric analysis (TGA, Fig. S12, SI). The TGA curve of NaAlg exhibited three main mass-loss events. The first stage, between 35 and 200 °C, involved an 11% mass loss, which is attributed to the removal of residual and structurally bound water, although it might also include partial decarboxylation of the alginate, as

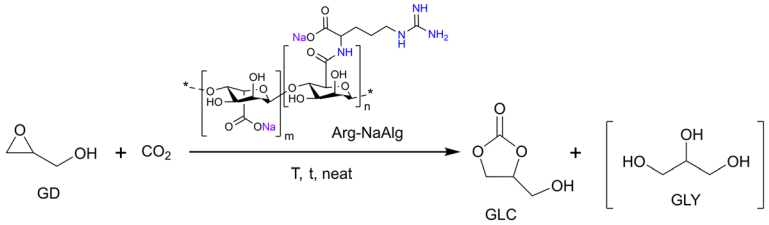

Scheme 4 Reaction scheme for the catalytic conversion of glycidol and carbon dioxide into glycerol carbonate. Glycerol can be formed as a side product in this reaction due to hydrolysis of glycidol in the presence of water, which is an impurity in commercial glycidol (see Table S1, SI).

previously reported.[20] The second stage, from 200 to 500 °C, accounted for 55% mass loss and is consistent with thermal degradation of the anhydrous polymer backbone and possible formation of sodium carbonate (Na_2CO_3). The third stage, occurring between 500 and 800 °C, showed a further 16% mass loss, likely due to decomposition of Na_2CO_3 into sodium oxide (Na_2O) with concurrent release of CO_2.[59,60] In contrast, the TGA curve of Arg-NaAlg displayed two main thermal events. The first, between 35 and 200 °C, involved an 11% mass loss analogous to the one observed for NaAlg, and similarly was attributed to moisture removal and possible partial decarboxylation. The second event, occurring between 200 and 800 °C, resulted in a 79% mass loss and is consistent with cleavage of the amide bonds linking grafted arginine units to the NaAlg backbone, and the concomitant degradation of the polymer backbone.[59,61] These TGA results indicate that the grafted arginine and the polymeric alginate backbone of Arg-NaAlg are expected to be stable under the envisaged reaction temperature for the catalytic conversion of CO_2 and glycidol to glycerol carbonate (<100 °C).

Catalytic performance

Among the materials prepared by immobilizing amino acids on Na-Alg, the comprehensive characterization presented above showed that successful grafting was achieved in the case of Arg-NaAlg and Lys-NaAlg. Initial screening for the conversion of glycidol and CO_2 into glycerol carbonate (Scheme 4) under identical conditions (80 °C, 10 bar CO_2, 3 h) revealed that Arg-NaAlg and Lys-NaAlg exhibited relatively similar catalytic performance (compare entries 1 and 2 in Table 1 to data in Table S2 in the SI). However, due to the above-mentioned issues encountered during the upscaling of Lys-NaAlg, Arg-NaAlg was selected as the preferred catalyst for detailed evaluation. When the test was carried out for 3 h at 80 °C, with a 3 wt% catalyst loading, the Arg-NaAlg catalyst achieved an excellent 92% NMR yield with nearly full selectivity (98%) towards glycerol carbonate (see Table 1, entry 1; isolated yield: 77%, see Fig. S18 in the SI). Under the same conditions, the homogeneous Arg-COOMe catalyst also displayed high conversion, affording 96% yield with 97% selectivity towards glycerol carbonate (Table 1, entry 4), whereas the pristine NaAlg provided only low glycerol carbonate yields (Table 1, entry 9). These results demonstrate that the arginine scaffold, with its basic sites and hydrogen-bonding moieties, constitutes an efficient catalyst for the cycloaddition of CO_2 to glycidol, both in its homogeneous and heterogeneous forms. Since the conditions in these initial tests led to nearly full conversion of glycidol, they are less suitable for comparing the catalytic activity of the heterogeneous and homogeneous

Table 1 Catalytic activity of Arg-NaAlg in the conversion of CO_2 and glycidol to glycerol carbonate, compared with its homogeneous counterpart (Arg-COOMe) and with NaAlg

Entry	Catalyst	Loading[d] (wt%)	T (° C)	Yield (%)	Selectivity (%)	TON_{Arg}	$TON_{active\ sites}$	TOF[e] (h^{-1})
1[a]	Arg-NaAlg	3	80	92	98	230	72	24
2[b]	Arg-NaAlg	1.5	80	78	97	388	122	41
3[c]	Arg-NaAlg	1.5	60	15	99	71	22	7
4	Arg-COOMe	3	80	96	97	110	55	18
5	Arg-COOMe	1.5	80	95	97	213	106	35
6[c]	Arg-COOMe	0.05	80	18	>99	1135	567	189
7	Arg-COOMe	1.5	60	59	>99	120	60	20
8	Guanidine	1.5	60	80	>99	—	65	22
9	NaAlg	3	80	18	>99	—	14	5
10	NaAlg	1.5	80	11	>99	—	17	6

Conditions: 20 mmol glycidol (1.482 g), 10 bar CO_2, 3 h, 400 rpm. TON_{Arg} = moles of glycerol carbonate per mole of arginine after 3 h of reaction. $TON_{active\ sites}$ = moles of glycerol carbonate per mole of active sites after 3 h of reaction (see the Experimental section for further details). NMR yields were determined by using 1,2,4,5-tetramethylbenzene as an internal standard. [a] The catalytic test reported in this entry was done in quadruplicate. The average value of glycerol carbonate yield is reported. [b] The catalytic test reported in this entry was done in triplicate. The average value of glycerol carbonate yield is reported. [c] The catalytic test reported in this entry was done in duplicate. The average value of glycerol carbonate yield is reported. [d] Relative to glycidol. [e] $TON_{active\ sites}$ was used to calculate the TOF for the catalysts applied in our work.

systems. Therefore, the two catalysts were tested again with half of the loading (1.5 wt%). Under these conditions (80 °C, 10 bar CO_2, 3 h), the Arg-NaAlg catalyst still showed high performance, achieving 78% yield with 97% selectivity towards glycerol carbonate (Table 1, entry 2), while its homogeneous counterpart, Arg-COOMe, reached a higher yield (95%) with the same high selectivity (Table 1, entry 5).

To rationalize the catalytic performance of Arg-NaAlg, it is worth noting that each of the catalysts reported in Table 1 displays different types of basic active sites. More specifically, the active sites of the NaAlg support are sodium carboxylate (COONa) moieties, whereas those of Arg-COOMe are the basic α-amino and guanidino groups in their deprotonated form, but might also be the chloride anions if the α-amino and guanidino groups are in their protonated form. Our catalyst, Arg-NaAlg, combines the sodium carboxylate moieties and the guanidino groups (in non-chlorinated form, see XPS results in Fig. S8 and S9, SI), with the latter expected to be more active due to their higher basicity. The basic carboxylate groups of NaAlg have been reported to efficiently catalyze the conversion of glycidol and CO_2 into glycerol carbonate (84% yield) at a high catalyst loading of 10 wt% under 5 bar CO_2 in 24 h.[20] Notably, the lower glycerol carbonate yields observed for NaAlg alone (Table 1, entries 9 and 10) compared to the Arg-NaAlg catalyst (Table 1, entries 1 and 2) in our tests at 80 °C indicate that the stronger basicity (pK_a ~12.5, see Fig. 1)[41] of the guanidino groups of grafted arginine species are more active than the milder sodium carboxylate groups (pK_a ~4.4)[39] present in alginate in catalyzing the reaction through activation of the hydroxyl group of glycidol (Scheme 1). Therefore, it can be concluded that although Arg-NaAlg contains both COONa and guanidino active sites, the enhanced catalytic performance is mainly attributed to the guanidino groups.

While the yield and selectivity towards glycerol carbonate provide a straightforward accessible way to compare the performance of the different catalysts, further insights can be gained by considering the turnover numbers (TONs) achieved by the different catalysts within the chosen reaction time (3 h). However, this a challenging task because the nature of the active sites differs among the catalysts. To reflect such complexity, we chose to define two types of TON, which are $TON_{activite\ sites}$ (based on the moles of all active sites) and TON_{Arg} (based on the moles of arginine units); see section S1 of the SI for further details. Each of the two provides different information, as there are 2 amino active sites per arginine in Arg-COOMe; 1 amino active site and 1 carboxylate active site per grafted arginine unit and 1 carboxylate active site per ungrafted NaAlg unit in Arg-NaAlg; and 1 carboxylate active site per monomer unit in NaAlg.

For the arginine-containing catalysts, TON_{Arg} was used as the basis for comparison. At first inspection, the heterogeneous Arg-NaAlg catalyst appears more active than the homogeneous Arg-COOMe, as reflected by its higher TON_{Arg} values (Table 1, entries 1 and 2 *vs.* 4 and 5). This observation seemingly contradicts the general trend that homogeneous catalysts exhibit higher intrinsic activity than their heterogeneous analogues. The apparent inconsistency likely arises from comparing Arg-NaAlg at the rising portion of its substrate conversion profile with Arg-COOMe operating near the conversion plateau. To obtain a more reliable comparison, both catalysts were therefore evaluated at a lower temperature of 60 °C using 1.5 wt% catalyst loading (Table 1, entries 3 and 7). Under these conditions, the glycerol carbonate yield decreased substantially for both systems, but the reduction was more pronounced for Arg-NaAlg (from 78% at 80 °C to 15% at 60 °C, compare entries 2 and 3 in Table 1). Based on the tests at 60 °C, the TON_{Arg} values clearly indicate that the homogeneous Arg-COOMe is more active, delivering a TON_{Arg} of 120 (Table 1, entry 7), whereas the heterogeneous Arg-NaAlg shows a lower TON_{Arg} of 71 (Table 1, entry 3). This is also true when $TON_{active\ sites}$ is considered. To accurately compare the activity of catalysts containing different types of active site species as Arg-NaAlg and NaAlg, the TON per active sites ($TON_{active\ sites}$) was applied. When comparing Arg-NaAlg with NaAlg at either catalyst loading, the arginine-grafted catalyst clearly showed higher catalytic activity, exhibiting a five- to sevenfold larger $TON_{active\ sites}$ than the NaAlg support alone. This enhancement reinforces our previous conclusion that the basic sites introduced by the grafted arginine moieties are significantly more active than the carboxylate groups. This is further highlighted by the fact that when Arg-NaAlg and NaAlg produced similar yields of 15% (Table 1, entry 3) and 11% (Table 1, entry 10), respectively, at the same catalyst loading (1.5 wt%), Arg-NaAlg reached this conversion at a temperature that was 20 °C lower.

To further elucidate the catalytic contributions, we conducted control experiments at 60 °C under 10 bar CO_2 for 3 h using guanidine in the hydrochloride form (Table 1, entry 8). This compound contains only one of the two active sites in Arg-COOMe. Guanidine exhibited a slightly higher $TON_{active\ sites}$ (65) compared to Arg-COOMe (60). Moreover, the glycerol carbonate yield obtained with guanidine was 80%, suggesting that the reaction is nearing a plateau under the applied conditions. These observations suggest that the guanidino site is more active than the α-amino group in Arg-COOMe.

Next, we compared the catalytic performance of Arg-NaAlg to that of the state-of-the-art heterogeneous halide-free catalyst for the cycloaddition of CO_2 to glycidol into glycerol carbonate, which was prepared by immobilizing 1,5,7-triazabicyclo[4.4.0]dec-5-ene (TBD), a superbase, onto Merrifield resin (Scheme 1a).[14] It is worth noting that TBD@Merrifield and Arg-NaAlg were applied under different reaction conditions and reactor configurations (see data in Table S7 of the SI) and display different types and amounts (per unit mass) of active sites, making a direct comparison difficult. However, it is possible to conclude that Arg-NaAlg is competitive with respect to TBD@Merrifield, as it requires a much shorter reaction time (3 *vs.* 18 h) to achieve an almost equivalent yield (78 *vs.* 82%) at a slightly higher temperature and pressure (80 °C, 10 bar CO_2 *vs.* 70 °C, 5 bar CO_2). Similar considerations apply to the comparison with other halide-free heterogeneous catalysts in Table S7 (see the SI),[62–64] though it is worth noting that they

require higher reaction temperatures, and either longer reaction times or higher catalyst loading to afford comparable yields to Arg-NaAlg. The notable catalytic performance of Arg-NaAlg is ascribed to the combined presence of basic guanidino sites from grafted arginine and a biobased polymer support rich in mild basic sodium carboxylate (COONa) groups and hydrogen bond donor (–OH) functionalities, which can act as a cooperative catalytic environment (Scheme 1c). In addition, the amide linkages formed during grafting may provide additional hydrogen-bonding interactions that could assist substrate activation (Scheme 1c).

Catalyst recyclability

The stability and reusability of the Arg-NaAlg catalyst were evaluated by assessing its performance over successive catalytic runs. At first, recyclability tests were performed at a fivefold scale-up under optimized conditions (80 °C, 3 h, 50 bar CO_2) for four consecutive cycles (Arg-NaAlg_1a-u, 1b-u, 1b-d, see Fig. S15–S17 for the results and the detailed test conditions). Under these conditions, the catalyst was reusable but the glycerol carbonate yield declined by approximately 15–25% after each cycle, indicating a gradual deactivation. This may arise from hydrolysis of the amide linkage connecting arginine to the alginate backbone, as suggested by the reduced intensity of the amide carbonyl band at 1655 cm^{-1} in the FTIR spectrum (Fig. 4e). The concurrent decrease in intensity of peaks at 1400 and 1593 cm^{-1}, assigned to the C–O and C=O stretching of sodium carboxylate groups, respectively, also suggests partial decarboxylation of the alginate support. The latter phenomenon was observed in the past when investigating the catalytic performance of unfunctionalized calcium alginate for the cycloaddition of CO_2 to glycidol at 80 °C, although in that study NaAlg showed a significantly higher stability than its calcium-based analogue.[20] Additionally, the strongly basic guanidino groups in Arg-NaAlg may promote degradation by hydrolysis of the alginate backbone. Indeed, evidence of alginate chain hydrolysis was already apparent during the 16 h immobilization reaction in ammonium carbonate buffer (pH 8–9) conditions, under which base-catalyzed scission can occur.[57] The formation of shorter, more dispersible fragments was indicated by the pronounced decrease in the weight-average molecular weight dispersity index (*Đ*) measured by GPC (*vide supra*). These smaller chains may exhibit higher intrinsic activity due to greater accessibility of their active sites, but are more difficult to recover, which can contribute to the observed gradual loss of overall performance upon recycling.

Finally, XPS analysis was conducted on the spent Arg-NaAlg catalyst after 4 runs (Fig. S10, SI), to further elucidate structural changes induced by the reaction conditions. The survey spectrum showed an almost complete disappearance of Na, indicating the loss of sodium carboxylate (COONa) functionalities. In the O 1s region, the oxygen species assigned to C*OO*Na shifted by approximately +1 eV in binding energy and increased in relative intensity by nearly twofold, whereas the C 1s components corresponding to *C*–O and O–*C*–O decreased substantially (Tables S4 and S5). Notably, the C 1s signal corresponding to the carbon in O–*C*=O remained largely unchanged (Tables S4 and S5), indicating that the carboxyl carbons themselves were largely retained, while the loss of Na and shift in O 1s suggest conversion of COONa into neutral carbonyl-containing species (COOH or C=O), rather than being removed entirely from the polymer backbone. The FTIR spectrum of the spent catalyst supports this interpretation, showing not only attenuated bands characteristic of carboxylate groups (1400 and 1593 cm^{-1}) but also the appearance of a carbonyl band at 1736 cm^{-1} (Fig. 4e and S13). This newly observed band may arise from adsorbed glycerol carbonate residues (see Fig. S14 in the SI for comparison of the ^{1}H NMR spectra of glycerol carbonate and spent Arg-NaAlg catalysts) and/or from neutral carbonyl species formed following the loss of Na. Concurrently, the relative *C*–*C* contribution in the C 1s XPS signal increased, attributable to renormalization after Na loss and/or to polymer chain scission, as reflected by the proportional decrease in O–*C*–O and C–*O*–C species associated with the alginate glycosidic linkages (Tables S4 and S5). This structural degradation is consistent with the decrease in M_n and M_w values for Arg-NaAlg_1a-u relative to the pristine catalyst shown by GPC (Table S6, SI).

The elemental analysis and XPS data indicated a pronounced decline in N-containing species in the Arg-NaAlg catalyst upon recycling (Tables S3–S5). This, together with the loss/conversion of the basic COONa groups, contributes to the observed gradual deactivation and also rationalizes the reduced water solubility of the spent material. Collectively, the XPS, FTIR, and GPC analyses indicate loss of active sites and partial depolymerization of the alginate backbone during catalysis. The use of more robust crosslinked alginates[65] could be a way to bypass such stability limitations and provide ground for further catalyst engineering.

To evaluate to what extent the arginine moieties leached upon hydrolysis of the amide linkage connecting the amino acid to the alginate backbone can contribute to the observed catalytic performance, we carried out a control test with an amount of the homogeneous Arg-COOMe catalyst that should mimic the amount of arginine lost in each cycle. The glycerol carbonate yield obtained under these conditions was 18% (Table 1, entry 6), which is much lower than the 93% yield obtained by Arg-NaAlg under the same conditions (Table 1, entry 1). This test suggests that the leached species are not a major contributor to catalytic performance, which is thus mainly ascribed to the heterogeneous Arg-NaAlg catalyst.

Since the possible causes of deactivation described above are expected to be temperature dependent, we conducted another set of recyclability tests of Arg-NaAlg under milder reaction conditions (45 °C, 24 h, and 30 bar CO_2). The catalyst exhibited improved reusability, maintaining stable yields (43–44%) after a small drop from the first run (51% yield) (Arg-NaAlg_2a-d, Fig. 6). Nevertheless, a reduction in the intensity of the characteristic FTIR bands at 1653, 1593, and 1400 cm^{-1} was still observed after 4 runs (Fig. 4d), albeit

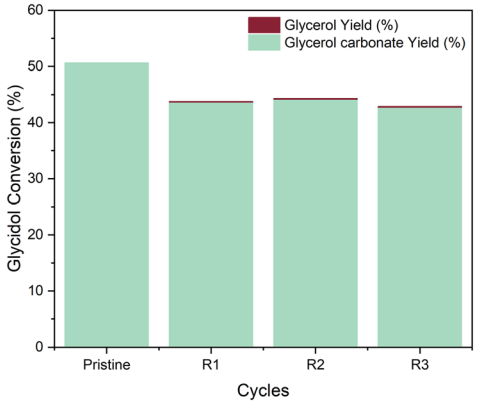

Fig. 6 Recyclability test of Arg-NaAlg_2a-d. Starting reaction conditions: 50 mmol glycidol (dried), 3 wt% catalyst, 45 °C, 24 h, 30 bar CO_2. For cycles R_1–R_3, the amount of glycidol and internal standard used was adjusted according to the amount of catalyst recovered after each cycle to keep the relative ratios of catalyst, glycidol, and internal standard constant. The CO_2 pressure was kept the same in all tests. The remaining catalyst mass after R_3 was 63.5% of the initial one.

to a lesser extent. GPC analysis further supports that the lower reaction temperature (45 °C) mitigates the risk of catalyst degradation, as the molecular-weight parameters (M_n and M_w) of the spent Arg-NaAlg_2a-d samples remained comparable to those of pristine Arg-NaAlg (Table S6, SI). Although the $Đ$ values of the spent catalysts ($Đ$ = 6–11 across four independent recyclability tests, see Table S6) were broadly similar to the pristine material ($Đ$ = 9), the samples recovered from reactions conducted at 80 °C (Arg-NaAlg_1a-u, 1b-u, 1b-d) consistently exhibited lower M_n and M_w values. This trend indicates that the higher temperature promotes partial degradation of the alginate backbone and/or the loss of grafted segments.

Conclusions

In this work, we report the novel design of a fully biobased, halide-free heterogeneous catalyst based on the immobilization of arginine, a naturally occurring amino acid with basic functionality, onto sodium alginate (NaAlg), a biopolymer derived from renewable sources (seaweed) that do not compete with the food industry. The immobilization was achieved *via* an amide coupling reaction and was monitored by FTIR, NMR, XPS, elemental analysis and GPC, which demonstrated successful amide bond formation and retention of functional groups. The obtained material (Arg-NaAlg) contains the basic sites provided by arginine together with the mild basic carboxylate groups of alginate. These basic sites can act as catalytic sites for an important reaction such as the conversion of the renewable resources carbon dioxide and glycidol (derived from biobased glycerol) into glycerol carbonate, which has a growing range of applications, spanning from polar solvent to monomer for the synthesis of polymers. The Arg-NaAlg catalyst achieved yields of up to 78% under mild conditions (80 °C, 10 bar, 3 h), with only 1.5 wt% catalyst loading, and nearly quantitative conversion to glycerol carbonate using 3 wt% catalyst. The performance of Arg-NaAlg is superior to that of previously reported biobased heterogeneous catalysts for this reaction and is competitive with that of the homogeneous counterpart (though the nature of the active sites differs) and with state-of-the-art heterogeneous catalysts. Moreover, the catalyst synthesis could be upscaled, and reusability tests demonstrated nearly constant glycerol carbonate yield over multiple cycles, albeit this required decreasing the reaction temperature to 45 °C. Overall, this study demonstrates a fully biobased, heterogeneous catalytic system for the synthesis of glycerol carbonate from glycidol and CO_2 that combines performance, recyclability, and sustainability.

Experimental

Materials

Sodium alginate (NaAlg), L-arginine methyl ester dihydrochloride (Arg-COOMe, $C_7H_{16}N_4O_2{\cdot}2HCl$, ≥98.0% purity), L-lysine methyl ester dihydrochloride (Lys-COOMe, $C_7H_{16}N_2O_2{\cdot}2HCl$, ≥99% purity), L-histidine methyl ester dihydrochloride (His-COOMe, $C_7H_{11}N_3O_2{\cdot}2HCl$, 97% purity), guanidine hydrochloride (guanidine, $CH_5N_3{\cdot}HCl$, ≥98% purity), 4-(4,6-dimethoxy-1,3,5-triazin-2-yl)-4-methyl-morpholinium chloride (DMTMM, 95% purity), ammonium carbonate ($(NH_4)_2CO_3$, ≥30% NH_3 basis), sodium hydroxide (NaOH, ≥98% purity), sodium nitrate ($NaNO_3$, ≥99.0% purity), glycidol (GD, 96% purity), glycerol carbonate (GLC, 94% GC purity), glycerol (GLY, ≥99.5% purity), methyl ethyl ketone (MEK, ≥99% purity), deuterium oxide (D_2O, 99.9 atom%) used for catalyst characterization, and dimethyl sulphoxide-d_6 (DMSO-d_6, 99.5 atom%) used for monitoring the catalytic reactions, were all purchased from Sigma-Aldrich. 1,2,4,5-Tetramethylbenzene (durene, >98.0% purity), as the internal standard, was purchased from Tokyo Chemical Industry (TCI). Ethylene glycol (EG, 99.9% purity) was purchased from VWR Chemicals. Hydrochloric acid (HCl, 37–38% w/w aqueous solution) and ethanol (technical grade, for washing) were purchased from Boom B.V. Acetone (technical grade) was purchased from Biosolve Chimie, and ethanol (absolute, for synthesis) from J.T. Baker. All chemicals were used without further purification.

Catalyst preparation

The synthesis of amino acids (AA) supported on sodium alginate (AA-NaAlg, with AA = Arg, His or Lys) was based on a procedure developed by Labre *et al.* for immobilizing amino acids on alginate oligosaccharides,[40] with slight alterations to adapt it to the amino acids and alginate used in this work. Initially, the AA-NaAlg materials were synthesized at the original scale used in the literature,[40] employing a 20 mL flat-bottom vial equipped with a cylindrical magnetic stirring bar. Next, the synthesis was upscaled to produce larger batches of the catalysts. For this purpose, the reaction was carried out in a 250 mL round-bottom flask equipped with an oval magnetic stirring bar.

The upscaled syntheses are described here in detail. 6 mmol (sodium uronate unit, 198.11 g mol^{-1}) of sodium alginate (NaAlg) were added to a magnetically stirred ammonium carbonate buffer (40 mL, 0.1 M, pH 9). The NaAlg was allowed to fully dissolve before the addition of an equivalent amount of amino acid methyl ester (6 mmol) and twice the amount of DMTMM (12 mmol), respectively. The reaction mixture was stirred for 16 h at 25 °C. Subsequently, an aqueous NaOH solution (60 mL, 1 M) was added to hydrolyze the methyl esters and the mixture was stirred for 2 h at 25 °C. The reaction mixture was then neutralized with a 1 M aqueous solution of HCl. The AA-functionalized NaAlg was then precipitated by adding the reaction mixture to absolute ethanol (900 mL). After 5 min, the precipitate was centrifuged (4 °C, 4000 rpm, 10 min) and then resolubilized in 50 mL of deionized water (or as much water as required to completely dissolve the precipitate). Absolute ethanol (900 mL) was added to the resolubilized mixture to precipitate the AA-functionalized NaAlg once again. The suspension was centrifuged to separate the solid product, which was then dried at 40 °C in a vacuum oven overnight (16–18 h) to remove residual water and ethanol.

Catalyst characterization

Elemental analysis (EA) of the biopolymer catalysts was conducted at the Mikroanalytisches Laboratorium KOLBE in Germany, using a Metrohm ion chromatograph model IC883Plus.

Fourier-transform infrared (FTIR) spectra were acquired over the range 4000–600 cm^{-1} on an IRTracer-100 spectrometer, with 64 scans averaged at a spectral resolution of 4 cm^{-1}.

The size of the synthesized catalysts was analyzed by gel permeation chromatography (GPC) on an Agilent Technologies 1200 series system equipped with three SUPREMA PSS columns (100 Å, 1000 Å, and 3000 Å; 300 × 8 mm, 10 μm) tempered at 40 °C and a refractive index detector. To minimize background noise, the catalysts (5–10 mg) were stirred overnight (16–18 h) at 25 °C in 1 mL of eluent (0.05 M aqueous $NaNO_3$) along with a drop of ethylene glycol, serving as the internal standard, to ensure dissolution. Before sample injection, the solutions were filtered through a 0.45 μm PTFE syringe filter. The samples (injection volume: 50 μL) were eluted with an aqueous solution of $NaNO_3$ (0.05 M) at a flow rate of 1 mL min^{-1}.

Nuclear magnetic resonance (NMR) spectra were measured on a Bruker BioSpin 600 MHz spectrometer. ^{1}H NMR spectra were recorded at 25 °C using 16 scans, a relaxation delay of 1 s, a pulse width of 12 μs, and an acquisition time of 2.75 s. ^{13}C NMR spectra were acquired at 25 °C using 1024 scans, a relaxation delay of 2 s, a pulse width of 10 μs, and an acquisition time of 0.92 s. To study the structure of Arg-NaAlg, an aliquot of the sample was dissolved under ambient conditions in 1 mL of D_2O, and 600 μL of this solution was used for measurement (25 mg for Arg-COOMe and DMTMM, 50 mg for NaAlg and Arg-NaAlg). For determining glycidol conversion and product yields after the catalytic tests, a small aliquot of the reaction solution was collected with a glass pipette and dispensed into an NMR tube. To facilitate the dispensing and to dilute the sample, 600 μL of DMSO-d_6 was dispensed through the pipette.

To determine the monomer ratio in sodium alginate (NaAlg), the ^{1}H NMR spectrum of 1% (w/v) NaAlg in D_2O was recorded on a Varian INOVA 500 MHz spectrometer at 90 °C. The standard parameters were 32 scans, a relaxation delay of 4 s, a pulse width of 3 μs, and an acquisition time of 4 s. The elevated temperature decreased the viscosity of the solution and facilitated separation of characteristic peaks corresponding to mannuronate and guluronate monomers, enabling accurate analysis of their relative abundance.

Thermogravimetric analysis (TGA) measurements were carried out under N_2 from 35 to 800 °C with a heating rate of 10 °C min^{-1} using a PerkinElmer thermogravimetric TGA-4000 analyzer.

X-ray photoelectron spectroscopy (XPS) analysis was carried out using a JEOL JPS-9010MC spectrometer equipped with twin anode X-ray sources (Al Kα and Mg Lα). Before measurement, the samples were kept overnight under high vacuum (10^{-8} mbar) in the pre-chamber to allow degassing. All samples were measured by using Al Kα (1486.6 eV) as X-ray probing radiation. The analyzed area of each sample was a circular spot with a diameter of 6 mm. The survey scan spectra were measured with a pass energy of 50 eV, a binding energy range of 0–1100 eV and energy step of 1 eV. The narrow scan spectra were measured with a pass energy of 10 eV and energy step of 0.1 eV. High resolution core spectra were fitted using synthetic Voigt function components, LF (a–e), with CasaXPS software (version 2.3.35PR1.0). All spectral energies were referenced to the binding energy of 284.8 eV of the sp^3 carbon synthetic component from the C 1s peak.

Catalytic tests

Cycloaddition of CO_2 to glycidol yielding glycerol carbonate. Before each reaction, the catalyst was pretreated at 60 °C overnight (16–18 h) to remove moisture. The catalytic tests were performed in a 10-block high-throughput reactor and a window reactor manufactured by Integrated Lab Solutions (ILS), located at the University of Groningen, the Netherlands (for more information, refer to previous reports).[66,67] In a typical reaction, glycidol (20 mmol, 1.482 g) and Arg-NaAlg (1.5 wt%, 22.23 mg) were added to a glass vial (46 ml, 30 mm outer diameter) along with a magnetic stirring bar. The vial cap contains an opening for a replaceable PTFE septum, which was then pierced with two needles to allow access to gaseous CO_2 (10 bar) during the reaction. Next, each glass vial was placed into the chosen reactor (10-reactor block or window reactor), and the reactor was then closed. Subsequently, the lines were flushed with N_2 (5 bar) 3 times and once with CO_2 (10 bar) before setting the pressure to a lower value than desired (<10 bar), and then the reactor was heated to 80 °C. If the desired pressure was not reached after reaching the desired temperature, the reactor was pressurized further until the target CO_2 pressure was reached. The reaction was then stirred at the set conditions for 3 h. After the set time, the stirring and heating were switched off, the reactor was cooled, opened, and the reaction vials were removed. The

internal standard, 1,2,4,5-tetramethylbenzene (durene, 1.5 mmol) and methyl ethyl ketone (3 mL, about twice the amount of glycidol) were added to the reaction solution, which was then stirred for 15 min (200 rpm). Then, the catalyst was allowed to settle at the bottom of the vial, and the reaction solution was sampled for NMR analysis in DMSO-d_6 (measured on a Bruker BioSpin 600 MHz spectrometer).

The yield and selectivity of glycerol carbonate (GLC) and mole balance of the cycloaddition reaction were calculated using the following formulas:

$$\text{Selectivity}_{\text{GLC}}\,(\%) = \frac{\text{mol}_{\text{GLC}}}{\text{mol}_{\text{GLC}} + \text{mol}_{\text{GLY}}} \times 100\%$$

$$\text{Yield}_{\text{GLC}}\,(\%) = \frac{\text{mol}_{\text{GLC}}}{\text{mol}_{\text{unreacted GD}} + \text{mol}_{\text{GLC}} + \text{mol}_{\text{GLY}}} \times 100\%$$

$$\text{Mole balance}\,(\%) = \frac{\text{mol}_{\text{unreacted GD}} + \text{mol}_{\text{GLC}} + \text{mol}_{\text{GLY}}}{\text{mol}_{\text{initial GD}}} \times 100\%$$

The moles of each relevant compound were calculated by integrating the respective peaks relative to those of the internal standard. The peaks chosen for NMR analysis comprised at least two peaks for each compound. These peaks were selected so as not to overlap with other peaks under any reaction condition. The peaks representing glycidol were at 2.68 and 2.98 ppm. The peaks of glycerol carbonate were at 3.51, 4.28, and 4.49 ppm, while the hydroxyl groups at 4.37 and 4.45 ppm of glycerol were used. The exact peak positions are taken from the reaction sample in DMSO-d_6. The use of an internal standard also enabled the calculation of the reaction mole balance, for which purpose both peaks of the internal standard were considered. The mole balance was in all cases in the range of 90–100%.

Selected tests were carried out in duplicate or triplicate, generally showing a high degree of reproducibility.

Recyclability tests. To ease catalyst recovery, two sets of conditions were employed in which the reaction was scaled up by a factor of 5 or 2.5 compared to the standard screening conditions: (1) glycidol (100 mmol, 7.408 g), 1.5 wt% Arg-NaAlg, 50 bar CO_2 at 80 °C for 3 h; (2) glycidol (50 mmol, 3.704 g), 3 wt% Arg-NaAlg, 30 bar CO_2 at 45 °C for 24 h. In subsequent runs, as catalyst losses exceeded 5%, the quantities of glycidol and internal standard were adjusted to keep the relative ratios of catalyst, glycidol, and internal standard constant. The pressure was either kept the same in all tests (option a) or adjusted to keep the glycidol-to-CO_2 ratio constant (option b). An additional parameter that was investigated was the use of dried (d) *vs.* untreated (u) glycidol. In summary, the following recycling conditions were tested: 1a-u, 1b-u, 1b-d, 2a-d. After the reaction, the solution was sampled for NMR analysis (see above in the description of a typical catalytic test), acetone (double the amount of glycidol) was added to the stirred reaction mixture to precipitate the spent catalyst. The sample was then centrifuged (4 °C, 10 000 rpm, 10 min) to separate the catalyst from the reaction mixture. The catalyst was then washed and centrifuged twice with ethanol and once with acetone before being dried overnight at 60 °C (16–18 h). The dried catalyst was weighed and used in the next cycle.

Author contributions

T. Kessaratikoon: conceptualization, data curation, formal analysis, investigation, methodology, visualization, writing – original draft, review & editing. S. Del Gobbo: data curation and formal analysis. V. D'Elia: conceptualization, funding acquisition, methodology, supervision, validation, writing – original draft, review & editing. P. P. Pescarmona: conceptualization, funding acquisition, methodology, project administration, resources, supervision, validation, writing – original draft, review & editing.

Conflicts of interest

There are no conflicts to declare.

Data availability

The data supporting this article have been included as part of the Supplementary information (SI): general information, experimental procedures, characterization data of pristine and spent catalysts including NMR, FTIR and XPS spectra, elemental analysis, GPC and TGA curves, recyclability investigation of the catalyst, and isolation of the glycerol carbonate product. See DOI: https://doi.org/10.1039/d5cy01517k.

Acknowledgements

T. Kessaratikoon acknowledges the Vidyasirimedhi Institute of Science and Technology (VISTEC) for an overseas research fund and the Srimedhi scholarship supporting her 24-month research stay at the University of Groningen under the supervision of Prof. Paolo Pescarmona. She further acknowledges the support of Prof. Paolo Pescarmona and the University of Groningen for providing laboratory facilities and materials essential for conducting the research.

References

1 M. O. Sonnati, S. Amigoni, E. P. Taffin De Givenchy, T. Darmanin, O. Choulet and F. Guittard, *Green Chem.*, 2013, **15**, 283–306.
2 P. P. Pescarmona, *Curr. Opin. Green Sustainable Chem.*, 2021, **29**, 100457.
3 M. A. Rasool, P. P. Pescarmona and I. F. J. Vankelecom, *ACS Sustainable Chem. Eng.*, 2019, **7**, 13774–13785.
4 P. Prete, S. Trano, P. Zaccagnini, L. Fagiolari, J. Amici, A. Lamberti, A. Proto, F. Bella and R. Cucciniello, *ChemSusChem*, 2024, **17**, e202401636.
5 *DAXSOL® Glycerol Carbonate*, https://ube.es/products/performance-chemicals/daxsol-glycerine-carbonate/, (accessed October 15, 2025).

6 R. Morales-Cerrada, B. Boutevin and S. Caillol, *Prog. Org. Coat.*, 2021, **151**, 106078.
7 M. Decostanzi, C. Bonneaud and S. Caillol, *J. Polym. Sci., Part A: Polym. Chem.*, 2019, **57**, 1224–1232.
8 T. Theerathanagorn, T. Kessaratikoon, H. U. Rehman, V. D'Elia and D. Crespy, *Chin. J. Chem.*, 2024, **42**, 652–685.
9 F. Magliozzi, G. Chollet, E. Grau and H. Cramail, *ACS Sustainable Chem. Eng.*, 2019, **7**, 17282–17292.
10 J. Sternberg and S. Pilla, *Green Chem.*, 2020, **22**, 6922–6935.
11 F. Yang, M. A. Hanna and R. Sun, *Biotechnol. Biofuels*, 2012, **5**, 13.
12 C. Muzyka, D. V. Silva-Brenes, B. Grignard, C. Detrembleur and J.-C. M. Monbaliu, *ACS Catal.*, 2024, 12454–12493.
13 P. Inrirai, J. Keogh, A. Centeno-Pedrazo, N. Artioli and H. Manyar, *J. CO2 Util.*, 2024, **80**, 102693.
14 N. Zanda, A. Sobolewska, E. Alza, A. W. Kleij and M. A. Pericàs, *ACS Sustainable Chem. Eng.*, 2021, **9**, 4391–4397.
15 H. Sun, Z. Lei, J. Shi and M. Jia, *Catalysts*, 2025, **15**, 668.
16 V. Aomchad, À. Cristòfol, F. D. Monica, B. Limburg, V. D'Elia and A. W. Kleij, *Green Chem.*, 2021, **23**, 1077–1113.
17 W. K. Teng, R. Yusoff, M. K. Aroua and G. C. Ngoh, *Sustainable Energy Fuels*, 2021, **5**, 274–282.
18 T. W. Turney, A. Patti, W. Gates, U. Shaheen and S. Kulasegaram, *Green Chem.*, 2013, **15**, 1925–1931.
19 A. Kostyniuk, D. Bajec, P. Djinović and B. Likozar, *Chem. Eng. J.*, 2020, **394**, 124945.
20 J. Poolwong, V. Aomchad, S. Del Gobbo, A. W. Kleij and V. D'Elia, *ChemSusChem*, 2022, **15**, e202200765.
21 A. J. Kamphuis, F. Picchioni and P. P. Pescarmona, *Green Chem.*, 2019, **21**, 406–448.
22 F. D. Monica and A. W. Kleij, *Catal. Sci. Technol.*, 2020, **10**, 3483–3501.
23 W. Natongchai, D. Crespy and V. D'Elia, *Chem. Commun.*, 2025, **61**, 419–440.
24 C. J. Whiteoak, A. H. Henseler, C. Ayats, A. W. Kleij and M. A. Pericàs, *Green Chem.*, 2014, **16**, 1552–1559.
25 Y. Wang and J. Duan, *ACS Appl. Polym. Mater.*, 2022, **4**, 5851–5860.
26 Z. Teng, Y. Tu, N. Jian, Q. Zhang, Y.-R. Lu, L. Li, Z. Cao, Y. Ao, M. Liu, Y. Yan, J. Wang, H. Wu, T. Ohno, J. Lu, C. Su and B. Liu, *Angew. Chem., Int. Ed.*, 2025, **64**, e202507654.
27 Z. Xu, K. Liu, H. Huang, Y. Zhang, Z. Long, M. Tong and G. Chen, *J. Mater. Chem. A*, 2022, **10**, 5540–5549.
28 F. Della Monica, A. Buonerba, A. Grassi, C. Capacchione and S. Milione, *ChemSusChem*, 2016, **9**, 3457–3464.
29 D. Jaraba Cabrera, L. Álvarez-Miguel, A. Hernando Rodríguez, A. Hamilton, M. E. G. Mosquera and C. J. Whiteoak, *Eur. J. Org. Chem.*, 2024, **27**, e202400219.
30 J. Rintjema, R. Epping, G. Fiorani, E. Martín, E. C. Escudero-Adán and A. W. Kleij, *Angew. Chem., Int. Ed.*, 2016, **55**, 3972–3976.
31 R. Huang, J. Rintjema, J. González-Fabra, E. Martín, E. C. Escudero-Adán, C. Bo, A. Urakawa and A. W. Kleij, *Nat. Catal.*, 2019, **2**, 62–70.
32 S. Sopeña, M. Cozzolino, C. Maquilón, E. C. Escudero-Adán, M. Martínez Belmonte and A. W. Kleij, *Angew. Chem., Int. Ed.*, 2018, **57**, 11203–11207.
33 C. J. Whiteoak, A. Nova, F. Maseras and A. W. Kleij, *ChemSusChem*, 2012, **5**, 2032–2038.
34 G. Fiorani, W. Guo and A. W. Kleij, *Green Chem.*, 2015, **17**, 1375–1389.
35 G. H. Kim and J. W. Yang, *J. CO2 Util.*, 2025, **101**, 103216.
36 C. Claver, M. B. Yeamin, M. Reguero and A. M. Masdeu-Bultó, *Green Chem.*, 2020, **22**, 7665–7706.
37 W. Jaroonwatana, S. Del Gobbo, V. D' Elia and D. Crespy, *Chem. Eng. J.*, 2024, **499**, 155635.
38 M. Toda, A. Takagaki, M. Okamura, J. N. Kondo, S. Hayashi, K. Domen and M. Hara, *Nature*, 2005, **438**, 178–178.
39 R. Abka-khajouei, L. Tounsi, N. Shahabi, A. K. Patel, S. Abdelkafi and P. Michaud, *Mar. Drugs*, 2022, **20**, 364.
40 F. Labre, S. Mathieu, P. Chaud, P.-Y. Morvan, R. Vallée, W. Helbert and S. Fort, *Carbohydr. Polym.*, 2018, **184**, 427–434.
41 F. A. Carey and R. M. Giuliano, *Organic Chemistry*, McGraw-Hill, 8th edn, 2011.
42 T. Tanaka, M. Noguchi, K. Watanabe, T. Misawa, M. Ishihara, A. Kobayashi and S. Shoda, *Org. Biomol. Chem.*, 2010, **8**, 5126–5132.
43 G. Kopplin, A. Lervik, K. I. Draget and F. L. Aachmann, *RSC Adv.*, 2021, **11**, 13780–13798.
44 C. A. Fitch, G. Platzer, M. Okon, B. E. Garcia-Moreno and L. P. McIntosh, *Protein Sci.*, 2015, **24**, 752–761.
45 N. Sahatsapan, T. Ngawhirunpat, T. Rojanarata, P. Opanasopit and P. Patrojanasophon, *AAPS PharmSciTech*, 2020, **21**, 212.
46 A. Heydari, N. Borazjani, F. Kazemi-Aghdam, J. Filo and I. Lacík, *Carbohydr. Polym.*, 2025, **348**, 122893.
47 G. Platzer, M. Okon and L. P. McIntosh, *J. Biomol. NMR*, 2014, **60**, 109–129.
48 O. Koniev and A. Wagner, *Chem. Soc. Rev.*, 2015, **44**, 5495–5551.
49 A. Artemenko, A. Shchukarev, P. Štenclová, T. Wågberg, J. Segervald, X. Jia and A. Kromka, *IOP Conf. Ser.: Mater. Sci. Eng.*, 2021, **1050**, 012001.
50 Z. Li, T. Li, J. Miao, C. Zhao, Y. Jing, F. Han, K. Zhang and X. Yang, *Sci. China Mater.*, 2023, **66**, 2290–2298.
51 F. Zažímal, S. Atri, D. Plašienka, L. Vrána, A. Stýskalík, A. Vlk, M. Čaplovičová, M. Šob, O. Monfort and T. Homola, *J. Mater. Chem. A*, 2025, **13**, 13909–13923.
52 X. Zhang and Y. Ding, *Materials*, 2022, **15**, 5844.
53 G. P. López, D. G. Castner and B. D. Ratner, *Surf. Interface Anal.*, 1991, **17**, 267–272.
54 J.-C. Dupin, D. Gonbeau, P. Vinatier and A. Levasseur, *Phys. Chem. Chem. Phys.*, 2000, **2**, 1319–1324.
55 J. S. Stevens, A. C. de Luca, M. Pelendritis, G. Terenghi, S. Downes and S. L. M. Schroeder, *Surf. Interface Anal.*, 2013, **45**, 1238–1246.
56 G. Hazarika, S. Das, A. Patel and D. Manna, *Environ. Sci.: Water Res. Technol.*, 2025, **11**, 691–701.
57 R. L. Whistler and J. N. BeMiller, *J. Am. Chem. Soc.*, 1960, **82**, 457–459.
58 P. Rosiak, I. Latanska, P. Paul, W. Sujka and B. Kolesinska, *Molecules*, 2021, **26**, 7264.

59 D. P. Valido, W. D. G. Júnior, M. E. de Andrade, A. A. Rezende, F. M. de Andrade de Carvalho, R. de Lima, G. das Graças Gomes Trindade, C. de Alcântara Campos, A. M. S. Oliveira, E. P. B. S. S. de Souza, L. A. Frank, S. S. Guterres, E. M. Sussuchi, C. R. S. Matos, A. Polloni, A. A. de Souza Araújo, F. F. Padilha, P. Severino, E. B. Souto and R. L. C. de Albuquerque Júnior, *Drug Deliv. Transl. Res.*, 2020, **10**, 1716–1728.

60 I. Quaratesi, P. Chipurici, V. Ferrara, C. Casas, A. Bacardit, N. Proietti, C. Talotta, C. Gaeta, V. Iuliano, I. Bruno, A. Pauciulo, R. Gliubizzi, I. Călinescu and E. Badea, *Green Chem.*, 2025, **27**, 10567–10581.

61 I. Corazzari, R. Nisticò, F. Turci, M. G. Faga, F. Franzoso, S. Tabasso and G. Magnacca, *Polym. Degrad. Stab.*, 2015, **112**, 1–9.

62 Z. Yue, T. Hu, H. Su, W. Zhao, Y. Li, H. Zhao, Y. Liu, Y. Liu, H. Zhang, L. Jiang, X. Tang, S. Shan and Y. Zhi, *Fuel*, 2022, **326**, 125007.

63 Y. He, X. Li, W. Cai, H. Lu, J. Ding, H. Li, H. Wan and G. Guan, *ACS Sustainable Chem. Eng.*, 2021, **9**, 7074–7085.

64 Z. Yue, T. Hu, W. Zhao, H. Su, W. Li, Z. Chen, Y. Chen, S. Li, L. Wang, Y. Liu, H. Zhang, S. Shan and Y. Zhi, *Appl. Catal., A*, 2022, **643**, 118748.

65 T. Behroozi Kohlan, Y. Wen and A. Finne-Wistrand, *Mater. Today Chem.*, 2025, **50**, 103196.

66 Y. A. Alassmy, Z. Asgar Pour and P. P. Pescarmona, *ACS Sustainable Chem. Eng.*, 2020, **8**, 7993–8003.

67 Y. A. Alassmy, P. J. Paalman and P. P. Pescarmona, *ChemCatChem*, 2021, **13**, 475–486.